Electrical Conductivity of Noble Gases at High Pressures

Article *in* Physical Review E · October 2007

DOI: 10.1103/PHYSREVE.76.036405 · Source: PubMed

6 authors, including:

John Adams
University of Colorado Colorado Springs
6 PUBLICATIONS **82** CITATIONS
SEE PROFILE

H. Reinholz
University of Rostock
110 PUBLICATIONS **2,213** CITATIONS
SEE PROFILE

R. Redmer
University of Rostock
257 PUBLICATIONS **7,255** CITATIONS
SEE PROFILE

V. Mintsev
Russian Academy of Sciences
143 PUBLICATIONS **1,680** CITATIONS
SEE PROFILE

Electrical conductivity of noble gases at high pressures

J. R. Adams
Institut für Physik, Universität Rostock, D-18051 Rostock, Germany
and School of Physics, University of Western Australia, Crawley WA 6009, Australia

H. Reinholz and R. Redmer
Institut für Physik, Universität Rostock, D-18051 Rostock, Germany

V. B. Mintsev, N. S. Shilkin, and V. K. Gryaznov
Institute of Problems of Chemical Physics, Russian Academy of Sciences, 142432 Chernogolovka, Moscow Region, Russia
(Received 30 April 2007; published 21 September 2007)

Theoretical results for the electrical conductivity of noble gas plasmas are presented in comparison with experiment. The composition is determined within a partially ionized plasma model. The conductivity is then calculated using linear response theory, in which the relevant scattering mechanisms of electrons from ions, electrons, and neutral species are taken into account. In particular, the Ramsauer-Townsend effect in electron-neutral scattering is discussed and the importance of a correct description of the Coulomb logarithm in electron scattering by charged particles is shown. A detailed comparison with recent experiments on argon and xenon plasmas is given and results for helium and neon are also revisited. Excellent agreement between theory and experiment is observed, showing considerable improvement upon previous calculations.

DOI: 10.1103/PhysRevE.76.036405 PACS number(s): 52.25.Fi, 52.27.Gr, 05.70.Ln, 72.15.Lh

I. INTRODUCTION

The conductivity of noble gas plasmas is of interest in relation to the metal-nonmetal transition at high densities. This transition occurs as pressure ionization gives rise to a sudden increase in the free electron density, which in turn results in a large increase in the electrical conductivity.

Investigation of noble gas plasmas has been conducted over the last 30 years using explosively driven shock wave plasmas, including He [1–3], Ne [4], Ar [4–6], Kr [7] and Xe [4,6,8–11]. In these experiments, ionization of a gaseous sample occurs through compression and heating behind the shock wave. Noble gas plasmas were created with temperatures T of $6000-10^5$ K and densities ρ of $0.001-10$ g/cm^3. The dc conductivity σ_{dc} was measured in each experiment. In the most recent experiments by Shilkin *et al.* [6], plasmas in magnetic fields have been investigated, providing measurements of the Hall voltage. Within the experimental temperature and density range, only partial ionization of the gas is achieved. A fundamental problem for plasma diagnostics is the determination of the free electron density n_{e}. Comparison between experimental measurements and theoretical predictions of transport properties can provide a useful diagnostic tool if we have a complete model of electron transport and if transport coefficients can be measured with sufficient accuracy.

In order to describe transport properties of dense plasmas, a consistent, quantum statistical description of electron motion is necessary. The cross sections for scattering of electrons by each species must be carefully calculated, while considering the influence of the surrounding medium. Transport properties of plasmas are heavily dependent on the state of the system, therefore an accurate picture of the plasma composition is also required.

In Sec. II, we present a linear response theory model of electron transport, which is able to take into account each of the above considerations. A brief overview of various approaches to calculating the scattering cross sections is given in Sec. III, as well as a discussion on the Ramsauer-Townsend effect [12,13] observed in noble gases.

In Sec. IV, results from linear response theory are compared in detail with recent experimentally determined dc conductivities of Ar and Xe plasmas. Experiments with He, Ne, and Kr plasmas are also discussed. Taking into account the Ramsauer-Townsend effect in the electron-neutral scattering leads to improvement on earlier results [14]. The plasma temperature and composition is required for theoretical calculations. Results of two different program packages for determining the plasma composition [15,16] are presented and discussed.

II. LINEAR RESPONSE THEORY

For a detailed discussion of plasma effects, we introduce the dimensionless parameters

$$\Gamma = \frac{e^2\beta}{4\pi\varepsilon_0}\left(\frac{4\pi n_{\mathrm{e}}}{3}\right)^{1/3},$$

$$\Theta = \frac{2m_{\mathrm{e}}}{\beta\hbar^2}(3\pi^2 n_{\mathrm{e}})^{-2/3},$$

where $\beta = 1/(k_{\mathrm{B}}T)$. The coupling parameter Γ is the ratio of the average potential energy to the temperature (in units of energy) and the degeneracy parameter Θ is the ratio of the temperature to the Fermi energy.

Linear response theory (LRT) in the formulation of Zubarev *et al.* [17] is a well-established general approach to electron transport in the presence of weak external fields. Electron motion is described using a linearized nonequilib-

rium statistical operator ϱ (NESO), and transport coefficients are expressed in terms of equilibrium force-force correlation functions (FFCFs). This approach is detailed thoroughly by Röpke [18], Reinholz [19], and Redmer [15] we give here only a brief outline.

Considering the influence of a weak external electric field $\boldsymbol{E}$ we presume that electron momentum, which determines the electric current, is a relevant observable. A set of $(L+1)$ generalized observables is defined. Each observable is the sum of electron momenta weighted by a different power n of the dimensionless energy

$$\boldsymbol{P}_n = \sum_k \hbar \boldsymbol{k} (\beta \epsilon_k)^n a_k^\dagger a_k, \tag{1}$$

where $\boldsymbol{k}$ is the wave vector, $\epsilon_k = \hbar^2 k^2/(2m_e)$ is the classical kinetic energy, and $a_k^\dagger a_k$ is the electron number operator. The generalized observables are referred to hereafter as *moments*. Time derivatives are taken with respect to the total electronic Hamiltonian $H = H_s + H_{ext}$:

$$H_s = \sum_k \epsilon_k a_k^\dagger a_k + \sum_{c,k,q} V^{ec}(q) a_{k+q}^\dagger a_k, \tag{2}$$

$$H_{ext} = e\boldsymbol{E} \cdot \boldsymbol{R}, \tag{3}$$

$$\dot{\boldsymbol{P}}_n = \frac{i}{\hbar}[H, \boldsymbol{P}_n] = \sum_c \boldsymbol{F}_n^{ec}, \tag{4}$$

$$\boldsymbol{F}_n^{ec} = \frac{i}{\hbar}[V^{ec}(q) a_{k+q}^\dagger a_k, \boldsymbol{P}_n], \tag{5}$$

where $V^{ec}(q)$ is the Fourier transform of the potential energy between electrons and species c, and $\boldsymbol{R}$ is the center of mass position of the electrons such that $\boldsymbol{P}_0 = im_e[H, \boldsymbol{R}]/\hbar$. A relevant statistical operator ϱ_{rel} is created assuming a maximum entropy condition, similar to the formation of the equilibrium statistical operator in the grand canonical ensemble [17]

$$\varrho_{rel}(t) = \frac{1}{Z_{rel}} e^{-\beta(H_s + \mu_e N_e + \Sigma_n \phi_n(t) \cdot \boldsymbol{P}_n)}, \tag{6}$$

where μ_e and N_e are the chemical potential and number of free electrons, respectively. Normalization $\mathrm{Tr}\{\varrho_{rel}\} = 1$ is ensured by the partition function Z_{rel}. The NESO $\varrho(t)$ satisfies a nonequilibrium von Neumann equation [15], in which correlations between particles are introduced through $\varrho_{rel}(t)$,

$$\frac{\partial \varrho(t)}{\partial t} - \frac{i}{\hbar}[H, \varrho(t)] = -\lim_{\varepsilon \to 0} \varepsilon[\varrho(t) - \varrho_{rel}(t)]. \tag{7}$$

Assuming small external fields, ϱ_{rel}, Eq. (6) is linearized,

$$\varrho_{rel}(t) = \varrho_0 \left(1 - \sum_n \boldsymbol{\phi}_n(t) \int_0^\beta d\tau e^{\tau H_s} \boldsymbol{P}_n e^{-\tau H_s} \right),$$

$$\varrho_0 = \frac{1}{Z_0} e^{-\beta(H_s + \mu_e N_e)},$$

and the Lagrange multipliers $\phi_n(t)$ are found by imposing the condition that ϱ_{rel} is sufficient to provide averages of all relevant observables

$$\langle \boldsymbol{P}_n \rangle^t = \mathrm{Tr}\{\varrho(t) \boldsymbol{P}_n\} = \mathrm{Tr}\{\varrho_{rel}(t) \boldsymbol{P}_n\}. \tag{8}$$

We proceed by solving Eq. (7) to obtain an expression for $\varrho(t)$ in terms of $\varrho_{rel}(t)$, and then solving Eq. (8) for the Lagrange multipliers $\phi_n(t)$. The dc conductivity σ_{dc} is determined by matching the phenomenological and statistical descriptions of the electric current density

$$\boldsymbol{j}(t) = \sigma_{dc} \boldsymbol{E} = -\frac{e}{\Omega_0 m_e} \langle \boldsymbol{P}_0 \rangle^t, \tag{9}$$

where Ω_0 is the normalization volume. An expression of the conductivity is found in terms of Kubo products N_{nm} and FFCFs d_{nm} [15,19,20]

$$\sigma_{dc} = -\frac{e^2 \beta}{\Omega_0 |d|} \begin{vmatrix} 0 & N_{0m} \\ \bar{N}_{n0} & d \end{vmatrix},$$

$$N_{nm} = \frac{1}{m_e} (\boldsymbol{P}_n; \boldsymbol{P}_m), \tag{10}$$

$$d_{nm} = \sum_c d_{nm}^{ec} = \sum_c \langle \boldsymbol{F}_n^{ec}; \boldsymbol{F}_m^{ec} \rangle,$$

where $N_{0m} = \{N_{00} N_{01} \cdots N_{0L}\}$ is a row vector, $\bar{N}_{n0} = \{N_{00} N_{10} \cdots N_{L0}\}^T$ is a column vector, and d is the $(L+1) \times (L+1)$ matrix with elements d_{nm}. Correlation functions of two observables A and B are defined by [17]

$$(A;B) = \frac{1}{\beta} \int_0^\beta d\tau \, \mathrm{Tr}\{\varrho_0 e^{\tau H_s} A e^{-\tau H_s} B\}, \tag{11}$$

$$\langle A;B \rangle = \lim_{\varepsilon \to 0} \int_{-\infty}^0 dt' e^{\varepsilon t'} (e^{iH_s t'/\hbar} A e^{-iH_s t'/\hbar}; B). \tag{12}$$

The Kubo products N_{nm} are generalized particle numbers given by [19]

$$N_{nm} = \frac{\Omega_0}{3\pi^2 \beta} \left(\frac{2m_e}{\hbar^2 \beta} \right)^{3/2} \left(n + m + \frac{3}{2} \right) F_{n+m+1/2}(\beta \mu_e), \tag{13}$$

where F_n are the Fermi integrals of order n,

$$F_n(\beta \mu_e) = \int_0^\infty dx x^n f_0(x), \tag{14}$$

and $f_0(x) = (\exp\{x - \mu_e \beta\} + 1)^{-1}$ is the Fermi distribution function of the normalized energy $x = \beta \epsilon_k$.

The FFCFs are expressed in terms of the momentum transfer (transport) cross sections $Q_m^{ec(l)}$ (see Sec. III) [19]. In the electron-ion (ei) FFCFs, collisions of electrons with ions of all charges $Z_j \equiv je$ are included,

$$d_{nm}^{\mathrm{ei}} = \frac{4\Omega_0 n_e}{3\beta}\sqrt{\frac{2m_e}{\pi\beta}}\int_0^\infty dx x^{n+m+2}e^{-x}\left(\sum_j \sqrt{n_j Q_m^{ej(1)}(x)}\right)^2, \tag{15}$$

where n_j is the density of ions with charge Z_j. The electron-neutral (ea) FFCFs are given by a similar expression

$$d_{nm}^{\mathrm{ea}} = \frac{4\Omega_0 n_e n_a}{3\beta}\sqrt{\frac{2m_e}{\pi\beta}}\int_0^\infty dx x^{n+m+2}e^{-x}Q_m^{\mathrm{ea}(1)}(x), \tag{16}$$

where n_a is the density of neutral particles. For electron-electron (ee) interactions, the FFCFs contain the higher order cross sections $Q_m^{\mathrm{ee}(l)}$ for $l=2,4,6,\ldots$,

$$d_{nm}^{\mathrm{ee}} = \frac{4\Omega_0 n_e^2}{3\beta}\sqrt{\frac{m_e}{\pi\beta}}\int_0^\infty dx x^3 e^{-x}\sum_l R_{nm}^{(l)}(x)Q_m^{\mathrm{ee}(l)}(x), \tag{17}$$

where $R_{nm}^{(l)}(x)$ are the polynomials [19]

$$R_{nm}^{(l)}(x) = R_{mn}^{(l)}(x),$$

$$R_{n0}^{(l)}(x) = 0, \quad R_{21}^{(2)}(x) = x + \frac{7}{2},$$

$$R_{11}^{(2)}(x) = 1, \quad R_{22}^{(2)}(x) = x^2 + 7x + \frac{77}{4}.$$

It is important to note that in Eqs. (10), all interactions within the plasma appear in an additive fashion within the FFCFs, $d_{nm}=d_{nm}^{\mathrm{ei}}+d_{nm}^{\mathrm{ea}}+d_{nm}^{\mathrm{ee}}$. Thus within LRT we have a clear and consistent structure in which to include all plasma species. This offers an advantage over other methods such as the relaxation time approximation (RTA), in which such a structure must be constructed, see, for example, Seeger [21] and Lee and More [22].

Convergence of the conductivity (10) occurs within LRT as the number of *moments* is increased [15,19]. For instance, 5% accuracy is achieved by using a two moment approximation while five moments give convergence better than 1%. This approach can be extended to describe other transport properties by considering other external perturbations. For example, inclusion of a temperature gradient allows calculation of the thermopower and heat conductivity [19,20].

These transport coefficients have previously been calculated within a three moment approximation using the FORTRAN90 program package COMPTRA04. Recently, however, the program ELECTRA07 has been developed, which allows transport coefficients to be calculated within a five moment approach, resulting in improved convergence [23]. In order to do this, higher order momentum transfer cross sections (see Sec. III) must be taken into account. Numerical improvements also allow for both more accurate and faster calculations. Furthermore, the inclusion of a magnetic field within ELECTRA07 enables calculation of the Hall resistivity [24,25]. The program package COMPTRA04 is nevertheless still employed for the calculation of the plasma composition.

III. SCATTERING MECHANISMS

Scattering of electrons from charged species is the most elementary collision within a partially ionized plasma (PIP). The dominant force is the Coulomb interaction, which is screened by other charged particles in the medium. We can treat electron-ion (ei) and electron-electron (ee) scattering in either the Born approximation, which assumes small angle scattering, or using a T-matrix (phase shift) approach, which also includes strong collisions. The momentum transfer cross sections are given by the collision integral

$$Q_m^{ec(l)}(k) = 2\pi\int_0^\pi d\theta \sin\theta(1-\cos^l\theta)\frac{\partial\sigma^{ec}}{\partial\Omega}. \tag{18}$$

In the Born approximation, the differential cross sections

$$\frac{\partial\sigma^{ec}}{\partial\Omega} = \left(\frac{\Omega_0 m_e}{2\pi\hbar^2}\right)^2\left(|V^{ec}(q)|^2 - \frac{\delta_{ec}}{2}|V^{ec}(q)V^{ec}(q')|\right) \tag{19}$$

depend on the interaction potential and

$$q = 2k\sin(\theta/2),$$

$$q' = 2k\cos(\theta/2), \tag{20}$$

which are the momenta transferred during scattering through angles of θ and $\pi-\theta$, respectively. If the bare Coulomb potential is introduced into the ei collision integral, then it becomes divergent and a cutoff value must be introduced for the maximum impact parameter. If on the other hand, we use the screened Coulomb (Debye) potential [26]

$$V^{ej}(r) = -\frac{Z_j e^2}{4\pi\epsilon_0 r}e^{-r/r_D}, \tag{21}$$

$$r_D = \sqrt{\frac{\epsilon_0}{\beta e^2\sum_j Z_j^2 n_j}},$$

where r_D is the Debye screening radius, the collision integral is convergent, and cutoff parameters are not required. The cross sections are written in terms of the corresponding Coulomb logarithms $\ln\Lambda$,

$$Q_m^{ec(l)}(k) = \left(\frac{Z_c e^2}{4\pi\epsilon_0}\right)^2\frac{\pi}{\epsilon_k^2}\ln\Lambda^{ec(l)}(k), \tag{22}$$

and the Coulomb logarithms required can be given analytically in terms of the parameter $b=4k^2r_D^2$ [27]

$$\ln\Lambda^{\mathrm{ei}(1)}(k) = \frac{1}{2}\left[\ln(1+b) - \frac{b}{1+b}\right],$$

$$\ln\Lambda^{\mathrm{ee}(2)}(k) = \left[1+\frac{3}{b}-\frac{1}{b(b+2)}\right]\ln(1+b) - \frac{5}{2}, \tag{23}$$

$$\ln\Lambda^{\mathrm{ee}(4)}(k) = 2\left(1+\frac{3}{b}+\frac{3}{b^2}\right)\left[\left(1+\frac{3}{b}+\frac{1}{b+2}\right)\ln(1+b) - 3\right].$$

In the T-matrix approach, the differential cross sections are given by the scattering amplitude $f(k,\theta)$ [28,29]

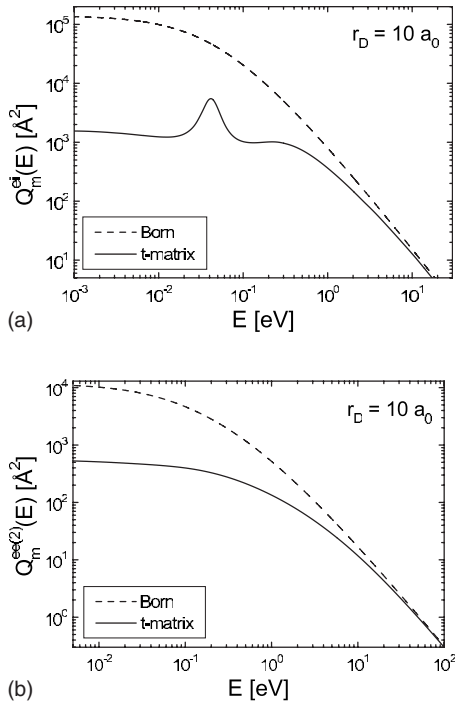

FIG. 1. Momentum transfer cross sections in dependence of energy for ei scattering (a) and ee scattering (b). Shown are results of the T-matrix (27) and the Born approximation (23), using a Debye screened potential.

$$\frac{\partial \sigma^{ec}}{\partial \Omega} = |f(k,\theta)|^2 - \frac{\delta_{ec}}{2}|f(k,\theta)f(k,\pi-\theta)|. \tag{24}$$

The scattering wave function is decomposed into partial waves $u_\ell(r)$ with respect to the angular momentums ℓ using Legendre polynomials P_ℓ,

$$\sum_{\ell=0}^{\infty} \frac{u_\ell(r)}{r} P_\ell(\cos\theta) \propto e^{i\mathbf{k}\cdot\mathbf{r}} + \frac{f(k,\theta)}{r} e^{ikr}, \tag{25}$$

and determined by numerically solving the radial Schrödinger equation [30]

$$\left(\frac{\partial^2}{\partial r^2} + k^2 - \frac{\ell(\ell+1)}{r^2} - \frac{2m_e}{\hbar^2} V^{ec}(r)\right) u_\ell(r) = 0.$$

At distances much larger than the screening length, the numerical solution can be matched to the general solution

$$u_\ell(r) = \sqrt{r}[B_\ell(k) J_{\ell+1/2}(kr) + C_\ell(k) Y_{\ell+1/2}(kr)]$$

to obtain $B_\ell(k)$ and $C_\ell(k)$, where J and Y are Bessel functions of the first and second kind [31]. Comparing the scattering wave function to the asymptotic solution, we obtain the scattering phase shift $\delta_\ell(k)$,

$$u_\ell(r \to \infty) \propto \sin[kr - \ell\pi/2 + \delta_\ell(k)],$$

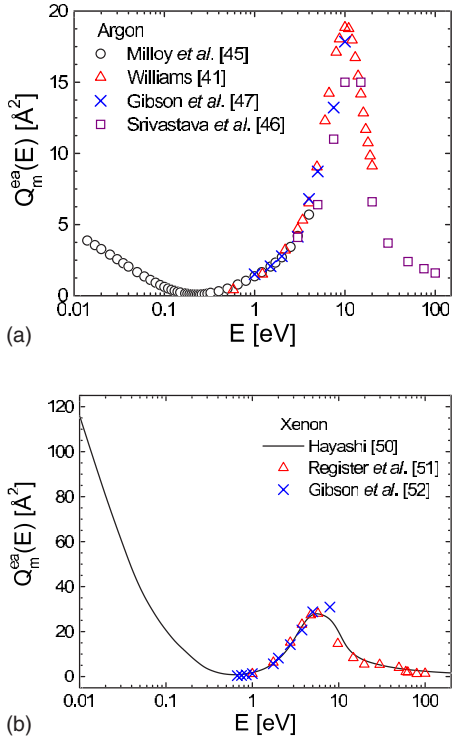

FIG. 2. (Color online) Experimental measurements of the ea momentum transfer cross sections as a function of energy for argon [42,46–48] (a) and xenon [51–53] (b). Note that Hayashi data is a fit to all available data up until 1983.

$$\delta_\ell(k) = \arctan\left(-\frac{C_\ell(k)}{B_\ell(k)}\right). \tag{26}$$

$\delta_\ell(k)$ is the change in phase due to the presence of the scattering potential. In order to include the effects of screening, the Debye potential (21) is used within the phase shift calculations. The momentum transfer cross sections are then calculated using the phase shifts [32,33]

$$Q_m^{ec(1)}(k) = \frac{4\pi}{k^2}\sum_{\ell=0}^{\infty}(\ell+1)\sin^2[\delta_\ell(k) - \delta_{\ell+1}(k)],$$

$$Q_m^{ee(2)}(k) = \frac{4\pi}{k^2}\sum_{\ell=0}^{\infty}\frac{(\ell+1)(\ell+2)}{2\ell+3}\sin^2[\delta_\ell(k) - \delta_{\ell+2}(k)],$$

$$Q_m^{ee(4)}(k) = \frac{4\pi}{k^2}\sum_{\ell=0}^{\infty}\frac{(\ell+1)(\ell+2)}{(2\ell+3)(2\ell+7)}\left\{\frac{(\ell+3)(\ell+4)}{2\ell+5}\sin^2[\delta_\ell(k) - \delta_{\ell+4}(k)] - \frac{2(2\ell^2+6\ell-3)}{2\ell-1}\sin^2[\delta_\ell(k) - \delta_{\ell+2}(k)]\right\}. \tag{27}$$

In Fig. 1, we compare the cross sections obtained using the Born approximation (23) with results from the T-matrix approach (27), applying the Debye potential to both. At high impact energies the T-matrix approach converges to the

TABLE I. Experimental densities ρ, temperatures T, and conductivities [6] σ_{exp}. Also presented are α: fraction of singly ionized atoms, σ: calculated conductivities, and Γ: Coupling parameter calculated using α_C. Subscripts C and Gr refer to results from the COMPTRA04 [54] and Gryaznov [16] composition programs, respectively. An asterisk indicates data obtained in reflected shock wave. Theoretical conductivities calculated within LRT, a five moment approximation with a T-matrix approach for ei and ee interactions, and experimental results for ea interactions. The number in square brackets denotes the power of 10.

	ρ (g/cm^3)	T (K)	α_C	α_{Gr}	σ_{exp} $(\Omega\ m)^{-1}$	σ_C $(\Omega\ m)^{-1}$	σ_{Gr} $(\Omega\ m)^{-1}$	Γ
Ar	2.53[−02]	7.85[+03]	5.64[−05]	6.38[−05]	8.80[+01]	1.33[+02]	1.46[+02]	9.54[−02]
Ar	2.54[−02]	8.18[+03]	9.34[−05]	1.06[−04]	1.60[+02]	1.91[+02]	2.11[+02]	1.08[−01]
Ar	2.56[−02]	9.38[+03]	4.43[−04]	5.01[−04]	7.70[+02]	5.60[+02]	6.13[+02]	1.59[−01]
Ar	2.57[−02]	9.82[+03]	7.17[−04]	8.20[−04]	7.20[+02]	7.71[+02]	8.48[+02]	1.79[−01]
Ar	2.59[−02]	1.05[+04]	1.40[−03]	1.61[−03]	9.40[+02]	1.20[+03]	1.32[+03]	2.10[−01]
Ar	2.62[−02]	1.11[+04]	2.37[−03]	2.76[−03]	1.24[+03]	1.66[+03]	1.84[+03]	2.37[−01]
Ar*	6.09[−02]	1.19[+04]	3.20[−03]	3.55[−03]	1.00[+03]	2.14[+03]	2.30[+03]	3.24[−01]
Ar*	6.22[−02]	1.27[+04]	5.58[−03]	6.24[−03]	2.20[+03]	3.04[+03]	3.28[+03]	3.68[−01]
Ar*	6.26[−02]	1.30[+04]	6.77[−03]	7.16[−03]	3.00[+03]	3.43[+03]	3.56[+03]	3.84[−01]
Ar*	6.34[−02]	1.34[+04]	8.64[−03]	9.24[−03]	3.11[+03]	3.99[+03]	4.17[+03]	4.06[−01]
Ar*	6.67[−02]	1.46[+04]	1.66[−02]	1.80[−02]	5.40[+03]	5.94[+03]	6.26[+03]	4.71[−01]
Ar*	6.77[−02]	1.49[+04]	1.93[−02]	2.09[−02]	6.03[+03]	6.51[+03]	6.86[+03]	4.88[−01]
Ar*	6.87[−02]	1.52[+04]	2.22[−02]	2.41[−02]	3.50[+03]	7.10[+03]	7.51[+03]	5.04[−01]
Ar*	7.30[−02]	1.63[+04]	3.58[−02]	3.70[−02]	1.20[+04]	9.18[+03]	9.33[+03]	5.62[−01]
Ar*	7.43[−02]	1.66[+04]	4.03[−02]	4.16[−02]	1.38[+04]	1.02[+04]	1.03[+04]	5.77[−01]
Xe	8.46[−02]	7.75[+03]	8.52[−04]	7.80[−04]	3.10[+02]	6.14[+02]	5.79[+02]	2.40[−01]
Xe	8.84[−02]	9.55[+03]	5.96[−03]	5.47[−03]	1.30[+03]	1.90[+03]	1.80[+03]	3.78[−01]
Xe	9.11[−02]	1.02[+04]	1.03[−02]	9.61[−03]	1.60[+03]	2.58[+03]	2.47[+03]	4.30[−01]
Xe	9.66[−02]	1.12[+04]	2.12[−02]	1.87[−02]	1.65[+03]	3.88[+03]	3.60[+03]	5.07[−01]
Xe	9.80[−02]	1.14[+04]	2.41[−02]	2.12[−02]	1.81[+03]	4.16[+03]	3.82[+03]	5.23[−01]
Xe	1.07[−01]	1.24[+04]	4.33[−02]	3.81[−02]	4.00[+03]	5.85[+03]	5.40[+03]	6.02[−01]
Xe	1.19[−01]	1.35[+04]	7.43[−02]	6.52[−02]	5.70[+03]	8.10[+03]	7.35[+03]	6.82[−01]
Xe*	2.34[−01]	1.29[+04]	4.93[−03]	3.66[−02]	5.26[+03]	7.07[+03]	5.77[+03]	7.84[−01]
Xe*	2.68[−01]	1.42[+04]	9.05[−02]	6.42[−02]	6.00[+03]	1.04[+04]	8.09[+03]	9.12[−01]
Xe*	2.87[−01]	1.48[+04]	1.15[−01]	7.77[−02]	1.00[+04]	1.20[+04]	9.45[+03]	9.70[−01]
Xe*	3.20[−01]	1.56[+04]	1.52[−01]	1.00[−01]	9.08[+03]	1.47[+04]	1.11[+04]	1.05[+00]
Xe*	3.29[−01]	1.57[+04]	1.58[−01]	1.06[−01]	1.63[+04]	1.51[+04]	1.16[+04]	1.06[+00]
Xe*	3.81[−01]	1.68[+04]	2.18[−01]	1.34[−01]	1.69[+04]	1.93[+04]	1.36[+04]	1.16[+00]
Xe*	4.53[−01]	1.83[+04]	3.07[−01]	1.88[−01]	2.39[+04]	2.51[+04]	1.79[+04]	1.27[+00]

analytic result of the Born approximation. At low impact energies, the T-matrix produces much smaller cross sections than the Born approximation. This is because the T-matrix approach gives a full description of strong collisions, which are important at low energies. The Born approximation is therefore not expected to be accurate for low temperature, high density plasmas, in which collisions with small impact parameters and low impact energies dominate.

In electron-neutral (ea) scattering, the dominant force is described by a dipole interaction, which is caused by the polarization of the atomic electron cloud as the scattering electron approaches. A polarization potential is commonly applied [34], which reads

$$V^{ea}(r) = -\frac{e^2}{8\pi\epsilon_0}\frac{\alpha_p}{(r^2+r_0^2)^2}\left(1+\frac{r}{r_D}\right)^2 e^{-2r/r_D}, \qquad (28)$$

where α_p is the electric polarizability of the neutral atom and r_0 ensures a finite interaction at zero separation. The latter is of the order of the size of the atom, see, e.g., Ref. [15] and references therein. This potential has been quite successful in describing the transport properties of metallic plasmas [35,36]. The polarization potential, however, is insufficient to describe scattering of electrons from the noble gas atoms. A feature known as the Ramsauer-Townsend minimum is observed in the cross sections of these atoms [12,13], which is a deep and broad minimum occurring at low impact energies

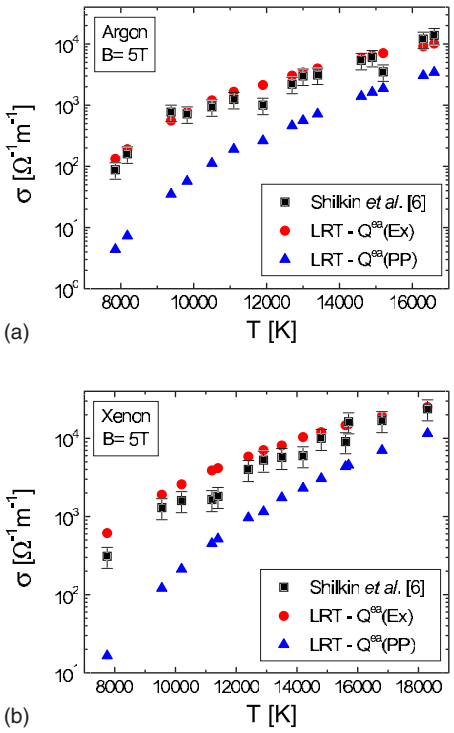

FIG. 3. (Color online) Conductivity of argon (a) and xenon (b) as a function of the temperature T, for plasma parameters see Table I. ■: experimental results [6] shown with 30% error bars. LRT calculated according to Eq. (10) using five moments, ei and ee collisions are treated using a T-matrix approach (27), ea interactions treated using experimental data ●, and a polarization potential (28) [14] ▲, respectively. Composition is obtained using COMPTRA04.

(~0.5 eV). This property cannot be reproduced using a polarization potential, and it has been shown in theoretical calculations that the exchange interaction of the scattering electron with the bound electrons must also be considered (see, for example, [37–39]).

In this work we use experimental results for the ea scattering cross section, He [40–43], Ne [42,44,45], Ar [42,46–48], Kr [49,50], and Xe [51–53]. As examples of the depth of the Ramsauer minimum we show experimental results for Ar and Xe in Fig. 2. Most of these experiments observe isolated scattering events, with no effects from a charged, surrounding medium. We therefore expect there to be medium corrections in using these results when the Debye length is small.

IV. COMPARISON WITH EXPERIMENTAL RESULTS

Initially, we concentrate here on conductivity measurements taken in shock compressed Ar and Xe plasmas [6], see Table I. Included are the experimentally measured conductivities, the mass densities and temperatures inferred from the shock wave and mass velocities (for details, see [6]) and theoretical calculations of the conductivity using a T-matrix approach for ei and ee interactions and experimental cross sections for ea interactions.

The plasma composition is required for theoretical calculations of the conductivity, we therefore present the compositions calculated using both the COMPTRA04 program [15,54] and the similar SAHA IV code [16,55] developed for partially ionized plasmas. Since, in these experiments, the fraction of doubly and higher charged ions is negligible, the composition is uniquely characterized by the ionization degree α, which represents the fraction of atoms that have been singly ionized. The ionization degree calculated for Ar plasmas using COMPTRA04 is consistently 3%–13% lower than that given by SAHA IV, resulting in 1%–9% smaller calculated conductivities. However, COMPTRA04 gives consistently higher ionization in Xe plasmas, in particular more than 25% in the case of high densities from the reflected shock wave conditions, resulting in up to 20% larger calculated conductivities. For the following calculations, we shall use the compositions calculated by COMPTRA04. Note that the conductivities calculated differ less than the ionization degrees and stay within the experimental errors.

The experiments produced plasmas with coupling parameters $0.1<\Gamma<2$ and degeneracy parameters $\Theta>5$ (not shown in Table I). Comparison with molecular dynamics simulations has shown that LRT is valid for $\Gamma \lesssim 1$ [56] and, since neither the T-matrix nor the ee FFCFs fully take into account the effects of degeneracy, LRT is valid only for nondegenerate to weakly degenerate plasmas ($\Theta \gtrsim 1$). The experiments shown in Table I therefore lie in a density and temperature range quite useful for the testing and comparison of theoretical approaches. In Fig. 3, we compare experimental results for the conductivity of Ar and Xe with theoretical calculations made using LRT within a five moment approach. Theoretical calculations using both experimental results for the ea cross sections and the polarization potential are shown.

Previous calculations within LRT by Kuhlbrodt *et al.* [14], in which the polarization potential (28) was used to calculate the ea cross sections Q_m^{ea} of noble gases, did not satisfactorily reproduce experimental results, as can be seen in Fig. 3. Since the Ramsauer minimum is not accounted for in these calculations, the contribution of the ea collisions is significantly overestimated, resulting in conductivities that are too low in comparison with the experimentally measured conductivities.

On the other hand, using experimental cross sections for the ea interactions, quite good agreement between theory and experiment is obtained. Theoretical results fall within the 30% error bars of the experimental results for many points. These results presented here therefore display a significant improvement in theoretical calculations of the conductivity of noble gas plasmas, matching theory and experiments satisfactorily.

Finally, we consider a wider range of experimentally available conductivities for noble gases, in a temperature and density region accessible to LRT. In Fig. 4, experimental results for the conductivity of He [1–3], Ne [4], Ar [4,6], and Xe [4,6,9] are shown. Most experimental points have error bars of around 30%, which are omitted here for the purpose of clarity. The calculations treat ei and ee interactions in a T-matrix approach using the Debye potential, while experimental momentum transfer cross sections are used for the ea interactions. Isotherms calculated within LRT are shown for He and Ne. From these we see how partial ionization can

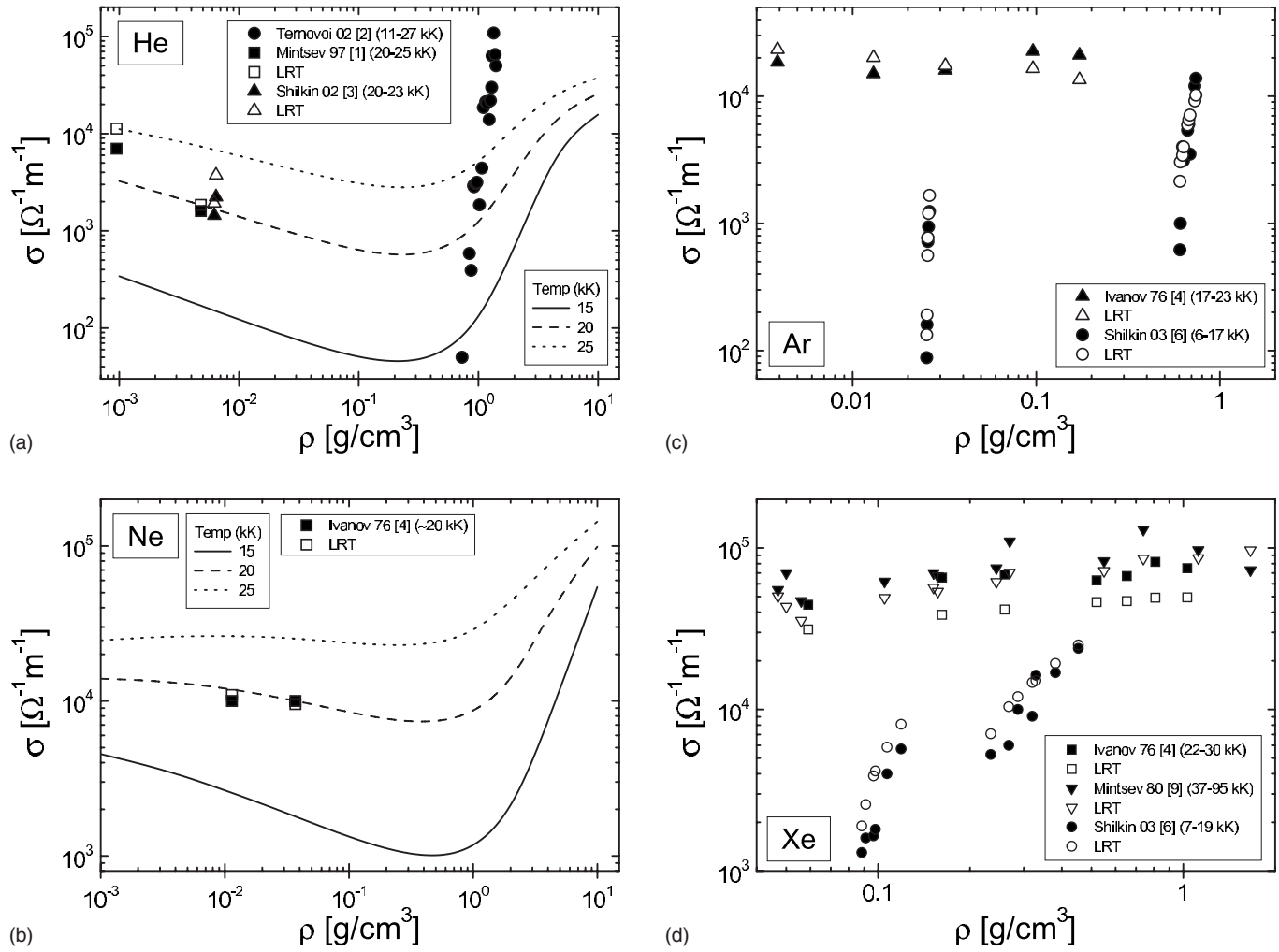

FIG. 4. Conductivity of helium, neon, argon, and xenon as a function of the mass density ρ: Experimental data from shock compressed plasma experiments. Results of LRT calculated using a five moment approximation, a T-matrix approach for ei and ee cross sections, and experimental results for ea cross sections. Composition is obtained using COMPTRA04.

introduce a minimum in the conductivity due to a reduction of free charge carriers and an additional scattering mechanism, as discussed in previous works [15,36]. Where the plasma temperature is available, we also give point by point comparison of LRT with each experimental point.

Overall, we obtain excellent agreement for all noble gases up to densities of $\rho \sim 1$ g/cm^3. Above this density, there are two factors that make calculations difficult. First, composition calculations for the heavier elements (Ar, Kr, Xe) become unreliable at larger densities, and also for temperatures below 10^4 K, due to instabilities in the solutions of the coupled mass action laws. For more details on this, see Kuhlbrodt *et al.* [14,36]. Second, at larger densities, diffraction of electrons from the ionic lattice should be considered and a static ionic structure factor S_{ii} must be taken into account within the FFCFs. The structure factor of dense plasmas has been calculated considering only elastic collisions, see Reinholz *et al.* [57]. However, in light of the previously mentioned difficulties in calculating the composition at large values of Γ, the structure factor for a randomly distributed system (S_{ii}=1) is applied in the present work. For these reasons, data at densities above 1 g/cm^3 [5,7,8,10,11] have been omitted in Fig. 4. In addition, quantum effects such as degeneracy, relevant at high densities, are not taken into account within the T-matrix approach.

V. CONCLUSIONS

LRT theory provides a quantum statistical framework within which all plasma interactions, including electron-electron interactions, as well as electron degeneracy and charge shielding can be accounted for in a consistent manner. For this reason, LRT is a well-suited theory for describing the partially ionized plasmas created in experiments. LRT also reproduces the known limiting cases. Analytical expressions within perturbation theory have been shown to be valid up to $\Gamma \sim 1$.

The ionization degree of a plasma is a crucial factor in determining which approximations can be made within theoretical models. In weakly ionized plasmas, particular emphasis must be placed on the description of ea collisions. In the case of noble gas plasmas, we find that a polarization

potential is insufficient to describe the Ramsauer-Townsend minimum, while experimental data for the momentum transfer cross sections can be easily incorporated into calculations. The T-matrix approach converges with the analytical results of the Born approximation at high energies, which can be applied to interactions between charged particles in high temperature, low density plasmas. Calculations using the Born approximation are very fast and are preferable to the T-matrix when appropriate. For most of the plasmas considered in this work, however, it is necessary to use a T-matrix approach to describe ei and ee interactions.

Sources of notable error can be found in both experiment and theory. The conductivity is measured under extreme conditions, placing significant strain on diagnostic equipment, and an error of 30% is suggested [6]. Measurements of pressure and temperature are also required from the experiments in order to calculate the composition, and each of these carries additional error. Then, using the same pressure and temperature as input, compositions determined using different thermodynamic models differ by a factor of up to 2.

Considering current experimental error and uncertainty in the composition, our present calculations within LRT provide excellent agreement over a wide range of temperatures $10^4\ \mathrm{K} \leq T \leq 10^5\ \mathrm{K}$ and densities $0.001\ \mathrm{g\ cm^{-3}} \leq \rho \leq 1\ \mathrm{g\ cm^{-3}}$, for all of the noble gas plasmas investigated. This represents enormous progress in dense plasma diagnostics.

We would like to thank G. Röpke for stimulating discussions and helpful comments. This work was completed with support of the German DFG, to the Graduiertenkolleg GK 567 and the Sonderforschungsbereich SFB 652, the Russian Science Support Foundation (CRDF), the Russian Ministry of Science and Education Grant No. Y2-P-11-17, and the President of the Russian Federation Grant No. MK 5782.2006.8.

[1] V. B. Mintsev, *Habilitation* (Institute of Problems in Chemical Physics, Chernogolovka, Russia, 1997).
[2] V. Y. Ternovoi, A. S. Filinov, A. A. Pyalling, V. B. Mintsev, and V. E. Fortov, in *Shock Compression of Condensed Matter*, edited by M. D. Furnish, N. N. Tadhani, and Y. Horie (AIP, New York, 2002).
[3] N. S. Shilkin *et al.*, G. S. I. Ann. Rep. **7**, 15 (2002).
[4] Yu. L. Ivanov, V. B. Mintsev, V. E. Fortov, and A. N. Dremin, Zh. Eksp. Teor. Fiz. **71**, 216 (1976).
[5] L. A. Gatilov *et al.*, Zh. Prikl. Tekh. Fiz. **1**, 99 (1985).
[6] N. S. Shilkin, S. V. Dudin, V. K. Gryaznov, V. B. Mintsev, and V. E. Fortov, Sov. Phys. JETP **97**, 922 (2003).
[7] V. D. Glukhodedov, S. I. Kirshanov, T. S. Lebedeva, and M. A. Mochalov, Sov. Phys. JETP **89**, 292 (1999).
[8] V. B. Mintsev and V. E. Fortov, Sov. Phys. JETP **30**, 375 (1979).
[9] V. B. Mintsev, V. E. Fortov, and V. K. Gryaznov, Sov. Phys. JETP **52**, 59 (1980).
[10] V. D. Urlin, M. A. Mochalov, and O. L. Mikhailova, High Press. Res. **8**, 595 (1992).
[11] V. B. Mintsev *et al.*, in *Shock Compression of Condensed Matter*, edited by S. C. Schmidt *et al.* (AIP, Woodbury, NY, 2000).
[12] J. Townsend and V. Bailey, Philos. Mag. **43**, 593 (1922).
[13] C. Ramsauer and R. Kollath, Ann. Phys. **395**, 536 (1929).
[14] S. Kuhlbrodt *et al.*, Contrib. Plasma Phys. **45**, 61 (2005).
[15] R. Redmer, Phys. Rep. **282**, 35 (1997).
[16] V. K. Gryaznov, I. L. Iosilevskiy, and V. E. Fortov, Mekh. Tekh. Fiz. **3**, 70 (1973).
[17] D. N. Zubarev, V. G. Morozov, and G. Röpke, *Statistical Mechanics of Non-Equilibrium Processes* (Akademie-Verlag, Berlin, 1996).
[18] G. Röpke, Phys. Rev. A **38**, 3001 (1988).
[19] H. Reinholz, R. Redmer, and D. Tamme, Contrib. Plasma Phys. **29**, 395 (1989).
[20] F. E. Höhne, R. Redmer, G. Röpke, and H. Wegener, Physica **128A**, 643 (1984).
[21] K. Seeger, *Semiconductor Physics*, 6th ed. (Springer-Verlag, Berlin, 1997).
[22] Y. T. Lee and R. M. More, Phys. Fluids **27**, 1273 (1984).
[23] ELECTRA07 has been developed at Rostock University and is to be made freely available towards the end of 2007.
[24] J. Adams, H. Reinholz, R. Redmer, and M French, J. Phys. A **39**, 4723 (2006).
[25] J. R. Adams, H. Reinholz, R. Redmer, N. S. Shilkin, V. B. Mintsev, and V. K. Gryaznov, Contrib. Plasma Phys. **47**, 331 (2007)
[26] W. D. Kraeft, D. Kremp, W. Ebeling, and G. Röpke, *Quantum Statistics of Charged Particles* (Akademie-Verlag, Berlin, 1986).
[27] R. J. Munn, F. J. Smith, E. A. Mason, and L. Monchick, J. Chem. Phys. **42**, 537 (1965).
[28] J. R. Taylor, *Scattering Theory: The Quantum Theory of Nonrelativistic Collisions* (Wiley, New York, 1972).
[29] B. H. Bransden and C. J. Joachain, *Physics of Atoms and Molecules*, 2nd ed. (Prentice Hall, Englewood Cliffs, NJ, 2003).
[30] J. L. M. Quiroz González and D. Thompson, Comput. Phys. **11**, 514 (1997).
[31] M. Abramowitz and I. A. Stegun, *Handbook of Mathematical Functions with Formulas, Graphs and Mathematical Tables*, 9th ed. (Dover, New York, 1964).
[32] R. S. Devoto, Phys. Fluids **10**, 354 (1967).
[33] Note that the final phase shift $\delta_{\ell+2}$ appearing in $Q_{\mathrm{m}}^{\mathrm{ee}(4)}$ is written incorrectly as $\delta_{\ell+1}$ by Devoto [32].
[34] R. Redmer, T. Rother, K. Schmidt, W. D. Kraeft, and G. Röpke, Contrib. Plasma Phys. **28**, 41 (1988).
[35] S. Arndt, F. Sigerneger, F. Bialas, W. D. Kraeft, M. Luft, T. Meyer, R. Redmer, G. Röpke, and M. Schlanges, Contrib. Plasma Phys. **30**, 273 (1990).
[36] S. Kuhlbrodt and R. Redmer, Phys. Rev. E **62**, 7191 (2000).
[37] A. W. Yau, R. P. McEachran, and A. D. Stauffer, J. Phys. B **11**, 2907 (1978).
[38] R. P. McEachran and A. D. Stauffer, J. Phys. B **16**, 4023 (1983).
[39] R. P. McEachran and A. D. Stauffer, J. Phys. B **17**, 2507

(1984).
[40] R. W. Crompton, M. T. Elford, and A. G. Robertson, Aust. J. Phys. **23**, 667 (1970).
[41] H. B. Milloy and R. W. Crompton, Phys. Rev. A **15**, 1847 (1977).
[42] J. F. Williams, J. Phys. B **12**, 265 (1979).
[43] D. F. Register, S. Trajmar, and S. K. Srivastava, Phys. Rev. A **21**, 1134 (1980).
[44] A.G. Robertson, J. Phys. B **5**, 648 (1972).
[45] D. F. Register and S. Trajmar, Phys. Rev. A **29**, 1785 (1984).
[46] H. B. Milloy, R. W. Crompton, J. A. Rees, and A. G. Robertson, Aust. J. Phys. **30**, 61 (1977).
[47] S. K. Srivastava, H. Tanaka, A. Chutjian, and S. Trajmar, Phys. Rev. A **23**, 2156 (1981).
[48] J. C. Gibson, R. J. Gulley, J. P. Sullivan, S. J. Bruckman, V Chan, and P. D. Burrow, J. Phys. B **29**, 3177 (1996).
[49] J. P. England and M. T. Elford, Aust. J. Phys. **41**, 701 (1988).
[50] A. Danjo, J. Phys. B **21**, 3759 (1988).
[51] M. Hayashi, J. Phys. D **16**, 581 (1983).
[52] D. F. Register, L. Vuskovic, and S. Trajmar, J. Phys. B **19**, 1685 (1986).
[53] J. C. Gibson, D. R. Lun, L. J. Allen, R. P. McEachran, L. A. Parcell, and S. J. Bruckman, J. Phys. B **31**, 3949 (1998).
[54] S. Kuhlbrodt, B. Holst, and R. Redmer, Contrib. Plasma Phys. **45**, 73 (2005).
[55] V. E. Fortov *et al.*, J. Exp. Theor. Phys. **97**, 259 (2003).
[56] I. Morozov, H. Reinholz, G. Röpke, A. Wierling, and G. Zwicknagel, Phys. Rev. E **71**, 066408 (2005).
[57] H. Reinholz, R. Redmer, and S. Nagel, Phys. Rev. E **52**, 5368 (1995).